Hindawi
Advances in Materials Science and Engineering
Volume 2018, Article ID 3849867, 10 pages
https://doi.org/10.1155/2018/3849867

Research Article

Sodium Dodecyl Sulfate-Modified Fe_2O_3/Molecular Sieves for Removal of Rhodamine B Dyes

Adnan A. AbdulRazak[1] **and Sohrab Rohani**[2]

[1]*Department of Chemical Engineering, University of Technology, 52 AlSinaa Street, Baghdad, Iraq*
[2]*Department of Chemical and Biochemical Engineering, Western University, London, ON, Canada N6A5B9*

Correspondence should be addressed to Adnan A. AbdulRazak; adnansss2002@yahoo.com

Received 15 February 2018; Revised 17 April 2018; Accepted 30 April 2018; Published 23 May 2018

Academic Editor: Peter Majewski

Studying the removal of rhodamine B (RB) dye by using zeolite 13X molecular sieves supported by Fe_2O_3 nanoparticles (denoted as Fe_2O_3-13X) is the main objective of this study. Fe_2O_3-13X was synthesized and modified by the addition of sodium dodecyl sulfate (SDS). The prepared Fe_2O_3-13X was characterized by XRD, TEM, SEM, and zeta potential. The effects of the solution pH, SDS amount, contact time, initial dye concentration, and adsorbent dosage on the removal efficiency of RB were studied. A maximum removal efficiency of 99.3% was achieved. The adsorption equilibrium data of RB were fitted using the Freundlich model, yielding the maximum adsorption capacity of 89.3 mg/g. The findings revealed that the RB adsorption onto Fe_2O_3-13X modified with SDS (Fe2O3-13X-Ms) was described by a pseudo-second-order kinetic equation. The results reported in this paper indicate that a high RB removal percentage was attained by adding SDS to Fe_2O_3-13X.

1. Introduction

Recently application of nanoparticles has increased in wastewater treatment. These materials have been established due to their properties such as high potential for removal and recovery of the effluent from wastewater, large surface area to volume ratio, reuse, and low cost. A number of researchers have used these materials as adsorbent [1, 2] or photo catalyst [3] for removal of dyes and heavy metals.

Synthetic organic dyes and rhodamine B (RB), in particular, are commonly used in different industries—including food, textile, and leather—as a coloring agent. These dyes are usually water contaminants and are frequently found in industrial wastewater. It is difficult to remove these dyes because of their complex structure. Thus, they have a tendency to persist in the environment, making serious issues with the quality of water, leading to some public health problems [4, 5].

In the pertinent literature, a wide range of chemical, physical, and biological methods for removal of RB from wastewater have been investigated. These methods include chemical degradation [6], physical adsorption [7, 8], photo degradation [9], and biological degradation [10]. The most commonly used dye removal method is based on adsorption, due to its high potential for the removal of dyes from wastewater and the simplicity and flexibility of the design. In addition, it does not produce dangerous by-products. Magnetic adsorbents have been extensively used in environmental applications. These adsorbents combine the adsorption process with magnetic separation, and thus, they do not require common separation processes, like centrifuge, to separate the solid phase from the solution. Among its other advantages is its potential for processing a large volume of wastewater in a short time without producing dangerous contaminants like flocculants. Magnetization of activated carbon is an example of these adsorbents [11].

Zeolites are microporous and crystalline-hydrated aluminosilicates. Both synthetic and natural zeolites are commonly used in different fields, such as ion exchange, adsorption, and heterogeneous catalysis. Zeolites are a subgroup of a large class of molecular sieves. The framework of pure silica is neutral. A negative charge of the zeolite framework stems from the presence of AlO_4, which is

stabilized by cations. These cations can be replaced by other ions using ion exchange methods.

Magnetic zeolites can be prepared via different methods, such as precipitation of iron oxides over zeolite [12]. It is used for the removal of dyes, heavy metals, and as a catalyst [13–15]. Unmodified magnetic zeolite has low dye removal efficiency. However, when magnetic zeolite is modified with surfactant, the removal efficiency as well as its selectivity will increase. Modification of zeolite and magnetic zeolite with surfactant is preferred to other magnetic zeolite modification processes due to its high potential and easy and cost-effective processes.

Surfactants are surface-active substances comprising of a hydrophobic nonpolar tail and a polar hydrophilic head. According to the charge on their polar head, they can be classified as anionic, nonionic, cationic, and amphoteric. Authors of a significant number of extant studies have focused on using cationic surfactants for modification of zeolite and magnetic zeolite for removal of different types of effluents [16, 17]. Research efforts to modify magnetic zeolites using anionic surfactants to remove dyes have been limited.

The goal of this research was to study the effect of modified Fe_2O_3-13X using SDS for removal of RB and understand the properties and mechanisms of the removal process. To meet this objective, the effects of the solution pH, amount of SDS, initial dye concentration, and adsorbent dose were investigated using the batch experiment method.

2. Materials and Methods

2.1. Materials. Among the materials used in this work, zeolite 13X was purchased from Sigma-Aldrich, USA; ferric nitrate nonahydrate ($Fe(NO_3)_3{\cdot}9H_2O$) was supplied by J.T. Baker, USA; SDS was sourced from Sigma-Aldrich, USA; NaOH was purchased from Alphchem, Canada, ON; and rhodamine B from Acros, USA. The molecular formula of RB is $C_{28}H_{31}N_2O_3Cl$. It has a molecular mass of 479 g/mol, and the chemical structure shown in Scheme 1.

2.2. Preparation of Fe_2O_3-13X. Initially, zeolite 13X granules were dried at 70°C and crushed and sieved to obtain powder of 53 μ particle size or less. Next, 5 g of $Fe(NO_3)_3{\cdot}9H_2O$ was dissolved in 100 mL of distilled water. After that, 10 g of Z13X was added to the ferric nitrate solution under stirring for 48 hours, and the resulting iron metal exchange zeolite 13X (Fe-13X) was washed with distilled water. The resultant solid was separated and dried at 70°C for 2 hours.

The Fe-13X was treated with 100 mL of 0.5 M NaOH. The obtained Fe_2O_3-13X was neutralized using distilled water, dried at 70°C for 2 hours, and then calcinated at 550°C for 2 hours. The color of prepared Fe_2O_3-13X was red to reddish-brown.

2.3. Characterization Methods. The prepared Fe_2O_3-13X was characterized by TEM, XRD, and Zeta potential meter. A Philips CM10 TEM was used with an accelerating voltage of 100 kV. XRP was performed using Rigaku MiniFlex XRD, Cu Kα radiation ($\lambda = 0.1524$ nm) was at angles ranging from 5° to 80° (2θ), the surface areas of 13X and Fe_2O_3-13X were calculated from N2 adsorption isotherms by using the Brunauer–Emmett–Teller (BET) method, and a Zetasizer Nano ZS 3000 HAS (Malvern, Worcestershire, UK) was employed when measuring the zeta potential.

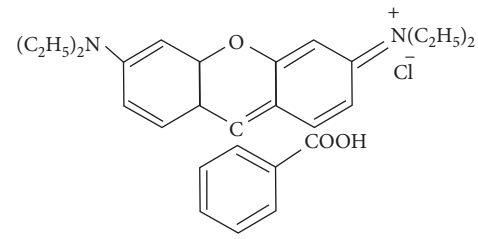

Scheme 1: The molecular structure of RB.

2.4. Adsorption Experiments

2.4.1. Batch Adsorption. RB adsorption experiments were conducted using a batch technique. First, 100 mg of adsorbent was shaken in 100 mL of RB with an initial concentration of 25 mg/L. Solution pH was adjusted to 3, and SDS was added to the dye solution at different amounts. The mixture was stirred until equilibrium was reached, the solid phase was removed by centrifugation, and the remaining dye concentration in the solution was measured using the UV-Vis spectrophotometer (Cary 60, Agilent Technology, Germany). The adsorbent amount was in the 250–1000 mg/L range, and the pH was varied from 3 to 9. The removal efficiency (%R) and the dye adsorption capacity (q) (mg/g) were calculated using the expressions below:

$$\%R = \frac{C_i - C_f}{C_i},$$
$$q = \left(\frac{C_i - C_f}{m}\right) * V, \quad (1)$$

where C_i and C_f are the initial and finial dye concentration (mg/L), respectively; V is the dye solution volume (L); and m is the adsorbent mass (g). Table 1 shows the batch removal experiments that were carried out in the different conditions.

2.4.2. Adsorption Isotherm. Adsorption isotherm, contact time, and kinetics study were conducted by using 100 mL of RB solution at an initial concentration (25 to 100 mg/L) with 1000 mg adsorbent, 100 mg SDS, and 3 pH in a 250 mL flask at 25°C. Aliquots were withdrawn at 10-minute intervals for investigation after centrifugation.

3. Isotherm and Kinetic Models

3.1. Isotherm Models. Equilibrium isotherms show the interaction between the adsorbates and the adsorbents and are thus important to optimize the application of the adsorbents. Langmuir and Freundlich models were fitted to the equilibrium experimental adsorption data. The Freundlich isotherm model assumes that distinctive locales are contained within a few adsorption energies, so it can be associated with nonideal adsorption occurring on heterogeneous surfaces [18]. The nonlinear form of this model is as follows:

Table 1: The variable values of batch adsorption process.

SDS mass (mg/L)	20	30	40	50	80	100	200	300
Adsorbent dose (mg/L)	200	400	600	800	1000	—	—	—
Initial RB concentration (mg/L)	25	50	75	100	—	—	—	—
pH of the solution	3	4	5	6	7	9	—	—

$$q_e = K_f C_e^{1/n}, \tag{2}$$

where q_e is the dye adsorption capacity at equilibrium (mg/g), C_e is the dye concentration at equilibrium (mg/L), $1/n$ is the factor of heterogeneity, and K_f is the Freundlich constant.

The above equation is linearized to evaluate the parameters of linear regression:

$$\log q_e = \left(\frac{1}{n}\right)\log C_e + \log K_f. \tag{3}$$

The main assumption of the Langmuir isotherm model is that the adsorbent surface is covered with a limited number of active sites, distributed in a homogeneous manner over the surface. It is given by the following nonlinear equation [19, 20]:

$$q_e = \frac{q_m K_L C_e}{1 + (K_L C_e)}, \tag{4}$$

where q_m is the maximum theoretical adsorption capacity (mg/g) and K_L is the Langmuir constant (L/mg). This model can be linearized in different forms and one of them is

$$\frac{C_e}{q_e} = \frac{C_e}{q_m} + \frac{1}{K_L q_m}. \tag{5}$$

The basic physical characteristics of Langmuir adsorption isotherm could be expressed as the dimensionless constant separation equilibrium parameter (R_L) that is determined by [21]

$$R_L = \frac{1}{1 + K_L C_i}, \tag{6}$$

where C_i is the initial RB concentration (mg/g) and R_L factor varies depending on the isotherm data. The calculated R_L values point to the isotherm type [22].

Commonly the tool used to compare between the models is R^2 (the coefficient of determination). Due to linearization (transformations), the present extreme points may perhaps disappear and be created by new points. For this reason, the best fitness should not depend only on R^2 [23, 24]. One of the proposed solutions to solve this problem is to minimize the sum squared error (SSE) between the experimental and predicted values using the Origin software:

$$\text{SSE} = \sqrt{\sum (Q_c - Q_e)^2}, \tag{7}$$

where Q_c and Q_e are the calculated and experimental values, respectively.

3.2. Kinetic Model. A study about the kinetic of RB adsorption on Fe_2O_3-13X is valuable because it provides information about the adsorption mechanism, which is necessary for selecting the optimum conditions for large-scale batch processes.

Generally, dye adsorption mechanism comprises of the following steps, whereby the slowest step or a combination of several steps determines the control rate of the sorption process:

(1) External mass transfer of molecules from the bulk solution to the boundary layer film surrounding the exterior surface of the adsorbent solid particles.

(2) Diffusion of the molecules through the boundary layer to the sites (external or internal) on the surface of the adsorbent. In this process, binding may be chemically or physically dependent on the energy. This step is usually assumed to be rapid.

(3) Adsorption of the molecules onto the adsorption site, after which they diffuse into the interior of the solid particles (intraparticle diffusion).

The adsorption mechanism of RB onto the Fe_2O_3-13X surface was investigated by the pseudo-first-order, pseudo-second-order, and intraparticle diffusion kinetics models.

In the pseudo-first-order model, the linear form is given by [25]

$$\ln(q_e - q_t) = \ln q_e - K_1 t, \tag{8}$$

where q_t is the actual dye concentration at time t (mg/g), q_e is the equilibrium RB concentration (mg/g), and K_1 is the pseudofirst-order rate constant, which is obtained from the linear plot $\ln(q_e - q_t)$ versus time.

The main assumption of a pseudo-second-order model is that the chemisorption of the adsorbate on the surface of adsorbents is the limiting step. The following equation can represent this model [26]:

$$\frac{t}{q_t} = \frac{1}{q_e} t + \frac{1}{K_2 q_e^2}, \tag{9}$$

where K_2 is the pseudo-second-order rate constant (g/mg/min), which was calculated by plotting t/q_t versus time (t).

The probability of the effect of adsorption of intraparticle diffusion was studied using the following model [27]:

$$q_t = K_3 t^{1/2} + C, \tag{10}$$

where K_3 is the intraparticle diffusion rate constant (mg/g/min$^{1/2}$).

4. Results and Discussion

4.1. Characterization of Synthesized Samples. Figure 1 shows the XRD patterns of Z13X and synthesized Fe_2O_3-13X. The diffraction maxima for Z13X at 2θ equal to 6.26°,

15.5°, 23.3°, 26.6°, and 31° corresponding to (111), (331), (533), (542), and (751) planes, respectively, are clearly observed in synthesized sample but with less intensity due to the overlapping of Fe_2O_3 reflection lines. This proves that the crystalline structure of Z13X is not damaged during the preparation steps. No peak due to Fe_2O_3 has been detected due to the lower crystallinity of Fe_2O_3-13X [28] and the dispersion of amorphous particles of Fe_2O_3 within the structure of Z13X [15].

The average crystallite size (D) was computed from the peak of high intensity at $2\theta = 35.7°$ using the Scherrer equation:

$$D = \frac{\lambda K}{\beta \cos 2\theta} \quad (11)$$

where D is the average crystallite size (nm), K is the Scherrer constant (0.9), λ is the wavelength of X-ray radiation applied (0.1540 nm), β is the full width at half maximum (FWHM) of diffraction (radians), and 2θ is the Bragg angle. The average crystallite size computed was 30 nm.

Figure 2 shows the micrograph of Fe_2O_3-13X, investigated by TEM. Approximately uniform black spherical particles with the average size of 9–49 nm could be observed, confirming the existence and precipitation of Fe_2O_3 particles. Due to the nanosize, as well as the high-speed movement of Fe_2O_3 nanoparticles during precipitation, the particles seem to collide with the surface and settle deeply through the zeolite softened material.

The SEM micrographs of 13X and Fe_2O_3-13X are shown in Figures 3(a) and 3(b), respectively. Figure 3(a) shows that the zeolite 13X particles form agglomerates consisting of nearly cubic-shaped grains of different sizes. Figure 3(b) shows the changes in the zeolite 13X particle morphology due to precipitation of magnetic particles. The image reveals that the zeolite 13X particles are covered by Fe-oxide clusters.

Table 2 shows the BET surface areas and pore volumes of 13X and Fe_2O_3-13X, and the results show that the surface area and pore volume of 13X were 573 m^2/g and 0.36 cm^3/g, while for Fe_2O_3-13X, 541 m^2/g and 0.21 cm^3/g. The decrease of the surface area of Fe_2O_3-13X can explain blocking of the microspore of 13X by the magnetic particles which decrease the pore volume of Fe_2O_3-13X compare to 13X.

4.2. Batch Adsorption Experimental Results

4.2.1. Effect of the Solution pH. The dye removal process is affected by the solution pH. The zeta potential of Fe_2O_3-13X and modified Fe_2O_3-13X-Ms at varying pH is shown in Figure 4. The positive values of the Fe_2O_3-13X zeta potential at pH values 3 and 4 changed to negative values after adding SDS.

The influence of the solution pH on the RB removal efficiency by Fe_2O_3-13X was studied at six pH values, ranging from 3 to 9, for the dye concentration of 25 mg/L in 1 L solution, with 1000 mg adsorbent, and using 100 mg SDS. As shown in Figure 5, the % removal efficiency changed significantly as the pH was increased from 3 to 9, having a maximum of 99.3% at pH 3, declining rapidly to 17% at pH 9.

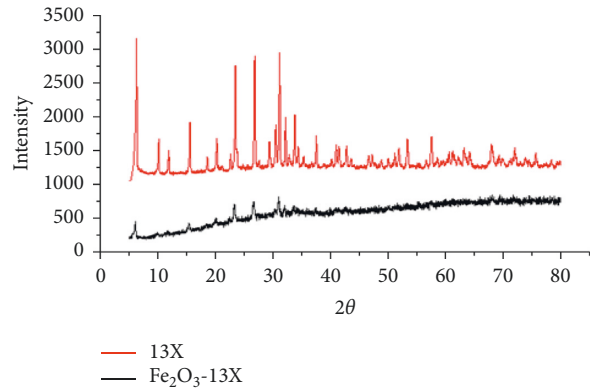

Figure 1: XRD patterns of Fe_2O_3-13X and Z13X.

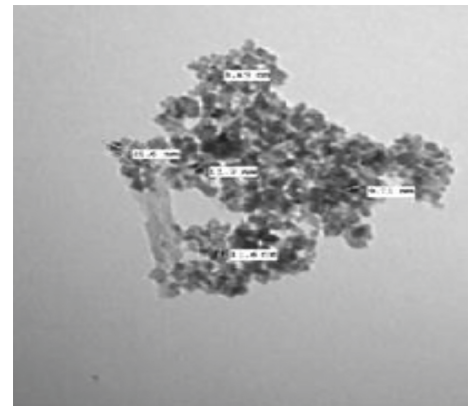

Figure 2: The TEM micrograph of Fe_2O_3-13X.

These results can be explained by the possible RB binding mechanism to the modified surface as shown in Figure 6. There are three different species of RB molecules depending on the pH of the solution (1) at pH > 4.0 zwitterion $RB^{\pm}$, (2) at pH > (1.0–3.0) RBH^+, and (3) at pH < 1.0 RBH_2^{2+} [29, 30].

At pH below 4.0, electrostatic interactions between the negatively modified surface of Fe_2O_3-13X and RBH^+ molecules will occur, contributing to the high dye removal percentage [31]. On the contrary, at pH above 4.0, the removal mechanism changes because of the formation of the zwitterion, and the combination effects of positive charge and negative charge of the RB molecules will affect the removal process [32]. Therefore, the binding of the dye molecules and the modified surface of Fe_2O_3-13X is reduced because of the repulsion force between the molecules of $RhB^{\pm}$ and the negative surface of the adsorbent. Consequently, the dye removal efficiency will decrease as the pH of the solution increase above 4. Similar results were reported by Jain et al. [4].

4.2.2. Effect of the Surfactant Amount. In micellization phenomena, surfactant molecules arrange themselves so that the nonpolar hydrophobic portions are shielded, forming the core, while the polar heads are located at the water-micelle interface touching the water molecules.

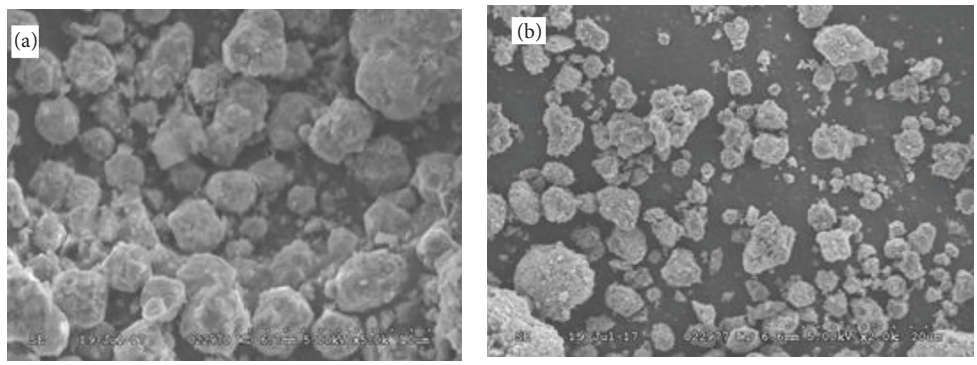

Figure 3: The SEM images of (a) 13X and (b) Fe_2O_3-13X.

Table 2: The texture properties of 13X and Fe_2O_3-13X.

Materials	BET surface area (m^2/g)	Average pore diameter (nm)	Pore volume (cm^3/g)
13X	573	2.3	0.36
Fe_2O_3-13X	541	2.6	0.21

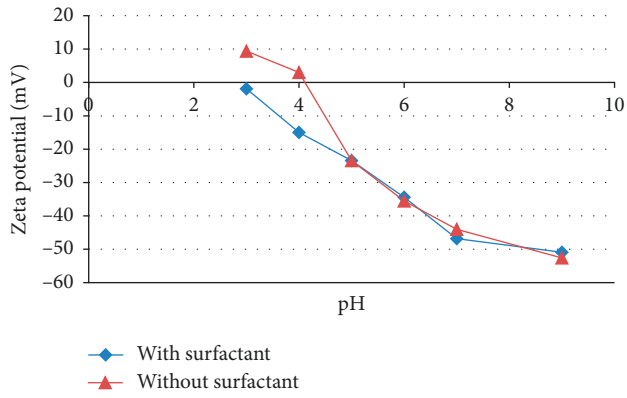

Figure 4: Zeta potential of Fe_2O_3-13X-Ms versus the solution pH.

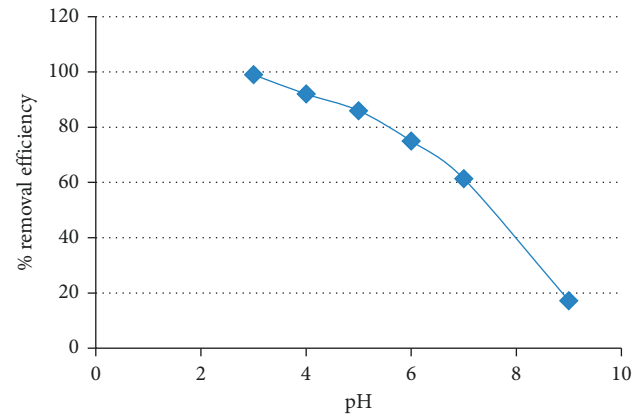

Figure 5: Removal efficiency as a function of the solution pH. Initial dye concentration = 25 mg/L, adsorbent dosage = 1000 mg/1 L solution, and SDS amount = 100 mg/1 L solution.

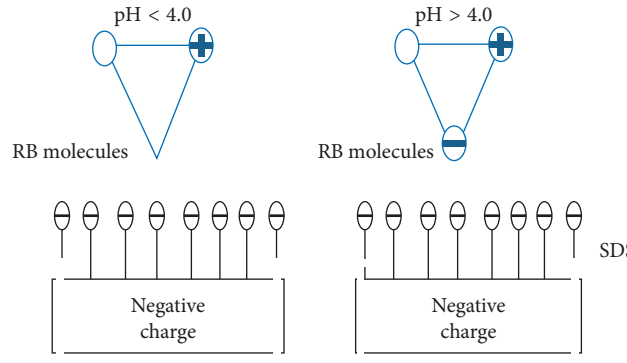

Figure 6: The suggested mechanism of RB binding to the modified surface.

Micellization occurs when the surfactant concentration is equal or less than its critical micelle concentration (CMC) at which micelles form. CMC of SDS was 230 mg/L [33]. In this work, sodium dodecyl sulfate (SDS) at concentrations below and above its CMC (i.e., 20, 30, 40, 50, 80, 100, 200, and 300 mg) was added to 1 L (25 mg/L initial concentration) dye solution, which was adjusted to pH 3 to investigate the effect of the surfactant amount on the % removal efficiency.

As shown in Figure 7, the % removal efficiency of RB by unmodified Fe_2O_3-13X at SDS = 0 was low (34%). However, when Fe_2O_3-13X was modified with anionic surfactant (SDS), the removal efficiency increased to 99.3%. This behavior might be explained as follows. Before adding the SDS to the solution, the repulsion force between the positive surface charge of Fe_2O_3-13X and the positively charged RB will decrease the % dye removal, while adding the SDS increased the dye removal efficiency in-line with the surfactant amount. The increase in %R can be explained as follows. At a solution pH of 3, the adsorbent surface had negative charge, like the charge of micelles. However, under these conditions, hydrophobic adsorption surface served as an appropriate substrate for adsorption of hydrophobic tail of the surfactant, creating a bilayer or monolayer with the negative sulfonate head in the direction of a solution [34].

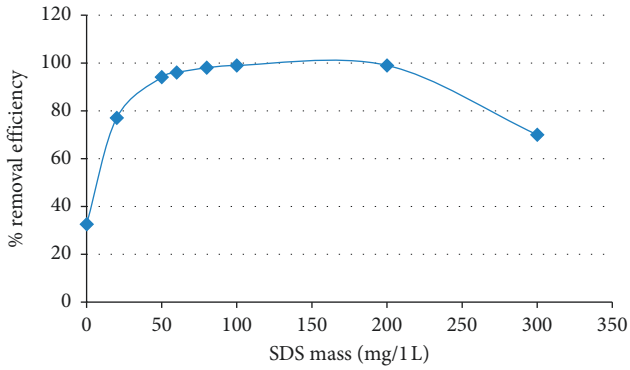

Figure 7: % removal efficiency versus SDS mass. Initial dye concentration = 25 mg/L, adsorbent dosage = 1000 mg/L solution, time = 60 min, and solution pH = 3.

This led to sorbate-sorbate associations, which contributed to increased adsorption [35]. A maximum %R was obtained at the SDS concentration of 100 mg/1 L solution. At higher SDS concentrations, RB adsorption decreased because of the aggregates of SDS in the solution, which can hinder the micelle formation on the adsorbent surface. Similar findings were reported by Shariati et al., who modified Fe_3O_4 nanoparticles with SDS and utilized it to remove safranin O [36].

4.2.3. Effect of the Adsorbent Amount. The adsorbent amount has an important effect on RB removal. The adsorbent amount was varied from 200 to 1000 mg/1 L solution, while the solution pH was fixed at 3, along with the initial dye concentration (25 mg/L), SDS amount (100 mg/L), and mixing time (1 hr). It can be seen from Figure 8 that the adsorbent amount increased the %R, likely due to the increased Fe_2O_3-13X surface area, or existence of a larger number of adsorption-active sites [37].

4.2.4. Effect of the Initial Concentration and Contact Time. As shown in Figure 9, the %R decreased from 99.3% to 87.5% as the initial RB concentration increased from 25 to 100 mg/L. This indicated that the dye adsorption onto the adsorbent depends on the initial RB concentration. At lower initial dye concentrations, higher surface area was available to the smaller number of RB molecules. Conversely, at higher dye concentrations, a large number of dye molecules interacted with the accessible adsorption sites.

Figure 9 shows the influence of initial concentration on the %R of RB. As seen from the graph, for all initial dye concentrations, removal was rapid during the first 10 minutes and attained equilibrium in 1 hour. This behavior may be attributed to the second-order type adsorption process, as will be discussed in the next section.

4.2.5. Effects of Ionic Strength. Wastewater from textile industries and dying process commonly contain other types of impurities such as alkali, salts, and acids, and the existence of these ions may compete with RB molecules on the

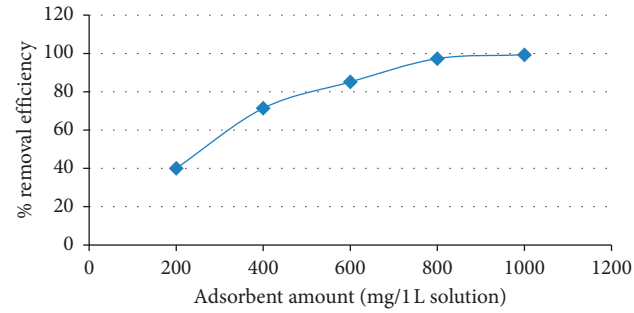

Figure 8: Removal efficiency versus adsorbent amount. Initial dye concentration = 25 mg/L, pH of the solution = 3, time = 60 min, and SDS amount = 100 mg/1 L solution.

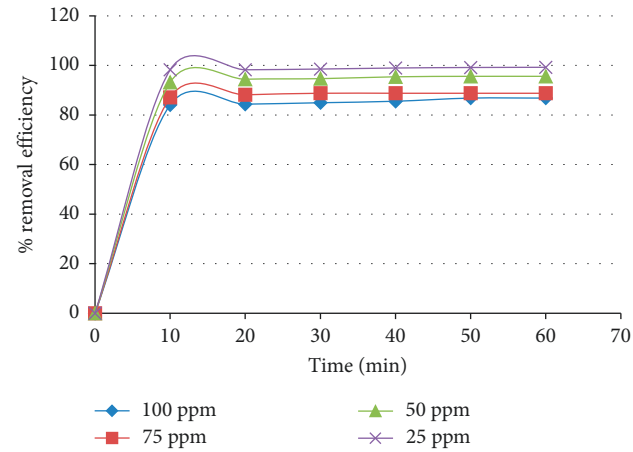

Figure 9: Removal efficiency versus contact time. Solution pH = 3, adsorbent dosage = 1000 mg/L solution, and SDS amount = 100 mg/L solution.

Table 3: Effect of ionic strength on the %RB removal.

% removal efficiency	NaCl concentration (mol/L)
99.3	0
97	0.001
95	0.01
92	0.05
87	0.1

adsorbent active sites. The effect of ionic strength on the RB removal onto Fe_2O_3-13X was investigated in the NaCl concentration in the range of 0.001 to 0.1 mol/L.

Table 3 shows the effect of NaCl concentration on the RB removal. The results illustrated that increasing salt concentration decrease the removal efficiency. This could be ascribed to the rivalry of Na+ ion and the positive charge of the dye (RB+) on the active sites on the adsorbent surface. Similar results were found by Shariati et al. [36].

4.3. Adsorption Kinetics. The isotherm experimental data for RB adsorption on Fe_2O_3-13X were tested with the Langmuir and Freundlich models. Table 4 shows the

Table 4: Nonlinear and linear Freundlich and Langmuir constants for the adsorption isotherm of RB on Fe_2O_3-13X-Ms.

	Freundlich parameters				Langmuir parameters			
	K_f (mg/g)	n	R^2	SSE	q_m	K_L	R^2	SSE
Linear method	38.9	3.6	0.99	73.362	89.3	0.63	0.96	493.2
Nonlinear method	37.61	3.25	0.983	94.64	83.8	0.7704	0.89	487.5

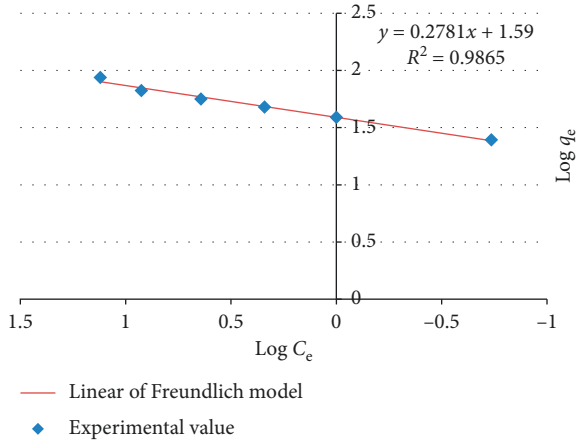

Figure 10: Freundlich isotherm of RB on Fe_2O_3-13X-Ms. Time = 60 min, pH of the solution = 3, and surfactant amount = 100 mg/L.

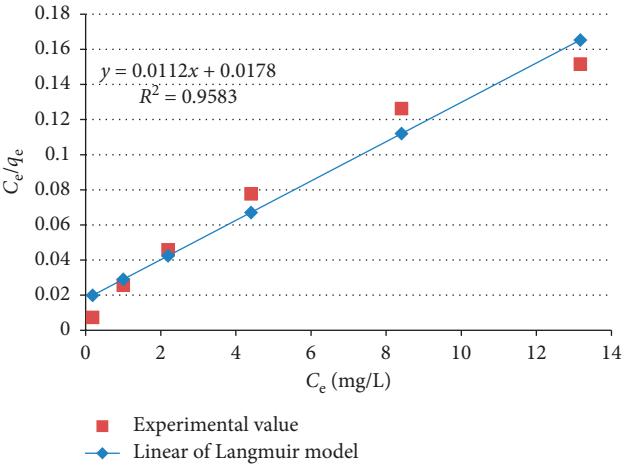

Figure 11: Langmuir isotherm of RB on Fe_2O_3-13X-Ms. Time = 60 min, pH of the solution = 3, and surfactant amount = 100 mg/L.

isotherm constants, correlation coefficients R^2, and SSE. Figure 10 shows a plot of different RB equilibrium concentrations (C_e) versus adsorption capacity (q_e) by using a linear form of the Freundlich model (3). The high R^2 value and low SSE value indicated that the linear form of the Freundlich model represents the experimental data. The value of $n > 1$ was satisfactory to direct toward favorable adsorption of RB by Fe_2O_3-13X material under test conditions [7].

Figure 11 shows the plots of the RB adsorption amount on the adsorbent (Fe_2O_3-13X-Ms) at different RB equilibrium concentrations (C_e) under the optimum conditions versus C_e/q_e using a linear form of the Langmuir isotherm model (5).

According to Table 4, the high value of SSE and low R^2 value indicate that the linear Langmuir model was not the suitable model to depict the adsorption phenomenon.

Our findings indicate that q_m at 25°C in the concentration range examined in this study was 89.3 mg/g. The R_L values for 25–100 mg/L RB dye concentrations varied from 0.059 to 0.0156, implying favorable adsorption.

Figure 12 shows the nonlinear isotherm of the Freundlich and Langmuir models for adsorption of RB on the adsorbent. The related parameters are shown in Table 4 for both models. The Freundlich model shows high R2 coefficient value and low SSE value compare to the Langmuir model. Therefore, again the results indicated that the nonlinear Freundlich isotherm model fits the experimental data, also the isotherm constants of nonlinear and linear form of the Freundlich model found close to each other.

So depending on the revealed results, it can thus be concluded that the adsorption isotherms of RB on the adsorbent can be fitted well by the nonlinear and linear

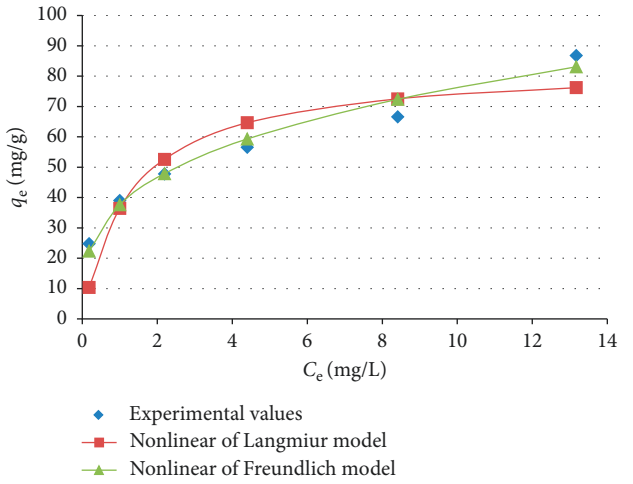

Figure 12: Nonlinear fitting of the Freundlich and Langmuir isotherm models of RB on Fe_2O_3-13X-Ms. Time = 60 min, pH of the solution = 3, and surfactant amount = 100 mg/L.

Freundlich model, demonstrating the (multilayer) heterogeneous adsorption characteristic.

A comparison of the results of the removal of RB by Fe_2O_3-13X-Ms with other reported adsorbents is given in Table 5. As shown in Table 5, the adsorbent employed in the present study exhibited good performance for the uptake of RB from wastewater.

4.4. Kinetic Model. The experimental kinetic data of adsorption of RB onto the modified Fe_2O_3-13X were fitted with

Table 5: Comparison of maximum adsorption capacity reported in extant studies with that of Fe_2O_3-13X-Ms.

Adsorbent	Maximum adsorption capacity (mg/g)	References
Kaolinite	46.08	[7]
Modified bentonite	142.8	[38]
Duolite C-20 resin	28.571	[39]
Mango leaf powder	3.31	[40]
Magnetic metal organic framework	28.36	[30]
Microwave-activated rice husk ash	21.89	[32]
Fe_2O_3-13X-Ms	89.3	This work

Table 6: Pseudo-second-order and intraparticle diffusion modelling results.

C_0 (mg/L)	Pseudo-second-order				Intraparticle diffusion		
	q_e (mg/g)	q_c (mg/g)	K_2 (g/mg/min)	R^2	C (mg/g)	K_3 (mg/g/min$^{1/2}$)	R^2
25	24.816	24.875	0.177	1	24	0.065	0.93
50	47.806	48.077	0.0555	1	45.9	0.26	0.93
75	66.589	66.67	0.0775	1	64.82	0.26	0.76
100	87.83	87.71	0.016	0.998	81.63	0.668	0.91

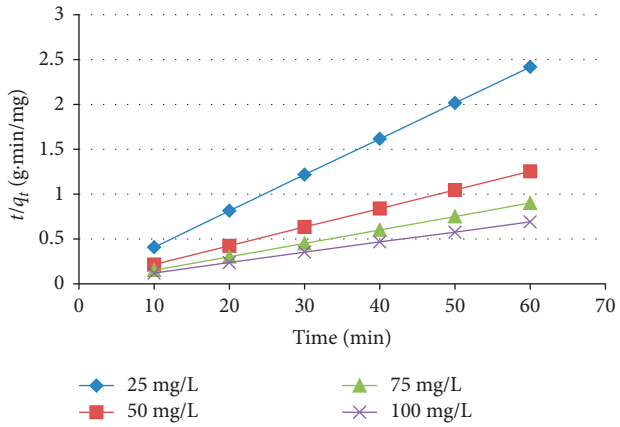

Figure 13: Pseudo-second-order model of RB adsorption onto Fe_2O_3-13X-Ms. Time = 60 min, pH of the solution = 3, and surfactant amount = 100 mg/L.

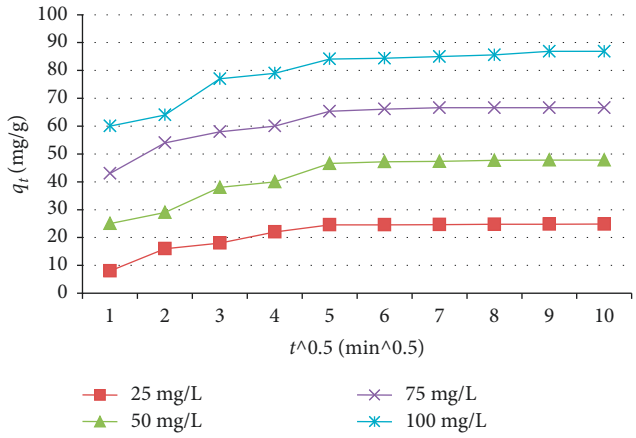

Figure 14: Intraparticle diffusion model for RB adsorption onto Fe_2O_3-13X-Ms. Time = 60 min, pH of the solution = 3, and surfactant amount = 100 mg/L.

the pseudo-first-order, pseudo-second-order, and intraparticle models. The results are shown in Table 6. In this work, for pseudo-first-order, the R2 value is low. This shows that the kinetics of adsorption of (RB) on Fe_2O_3-13X-Ms does not fit to the pseudo-first-order model.

Figure 13 shows the fitted linear plots of the pseudo-second-order model. From Table 6, the values of R2 are more than 0.998 for all initial dye concentrations. This approves that the adsorption kinetics of (RB) on Fe_2O_3-13X-Ms fits well to a pseudo-second-order kinetic model. Also, the values of adsorption capacity calculated by this model were close to the experimental values of adsorption capacity. This result confirms that the rate of RB adsorption over Fe_2O_3-13X may be controlled mainly by a chemisorption process and agrees with an earlier suggested mechanism obtained from the breakthrough curve of the RB removal [41].

Figure 14 shows the plots of the intraparticle diffusion model. It can be seen from this figure for all initial dye concentrations, there are two segments, each segment shows different mechanism of adsorption. In the first linear segment, the adsorption capacity changes fast with time until it reaches equilibrium; this indicates that the boundary layer diffusion may be the control step. While in the second segment, the experimental data points were the horizontal line which indicates that the equilibrium had been reached which indicate happening on the intraparticle diffusion. The calculated values of C, K_3, regression, and correlation constants are presented in Table 6. The nonappearance of such feature points to that the experimental data do not fit the intraparticle diffusion model because of low values of $R^2 \leq 93$, in comparison with the high values of R^2 estimated from the pseudo-second-order model and the intraparticle diffusion was not only the limiting control step. Moreover, the plot does not pass through the origin, indicating that the first stage of this plot involved boundary layer adsorption [42].

5. Conclusions

The SDS modified Fe_2O_3-13X was studied for the RB removal from aqueous solutions.

(1) The results clearly revealed that Fe_2O_3-13X-Ms is an active adsorbent for the removal of RB from aqueous solutions, as 99.3% removal was achieved using 100 mg/L SDS at pH 3 for an initial RB dye concentration of 25 mg/L and adsorbent amount of 1000 mg/L.

(2) The solution pH, surfactant amount, and adsorbent dosage highly effected the removal of dye by adsorption on Fe_2O_3-13X.

(3) Linear and nonlinear forms of the Freundlich isotherm model fitted equilibrium data of RB adsorption onto the Fe_2O_3-13X-Ms.

(4) The maximum adsorption capacity was found to be 89.3 mg/g.

(5) The pseudo-second-order kinetic model fitted the kinetic adsorption processes of RB well.

Data Availability

The data used to support the findings of this study are available from the corresponding author upon request.

Conflicts of Interest

The authors declare that they have no conflicts of interest.

References

[1] S. Zhang, H. Gao, J. Li et al., "Rice husks as a sustainable silica source for hierarchical flower-like metal silicate architectures assembled into ultrathin nanosheets for adsorption and catalysis," *Journal of Hazardous Materials*, vol. 321, pp. 92–102, 2017.

[2] S. Zhang, H. Yang, H. Huang et al., "Unexpected ultrafast and high adsorption capacity of oxygen vacancy-rich WOx/C nanowire networks for aqueous Pb2+ and methylene blue removal," *Journal of Materials Chemistry A*, vol. 5, no. 30, pp. 15913–15922, 2017.

[3] S. Zhang, H. Gao, X. Liu et al., "Hybrid 0D–2D nanoheterostructures: in situ growth of amorphous silver silicates dots on g-C3N4 nanosheets for full-spectrum photocatalysis," *ACS Applied Materials and Interfaces*, vol. 8, no. 51, pp. 35138–35149, 2016.

[4] R. Jain, M. Mathur, S. Sikarwar, and A. Mittal, "Removal of the hazardous dye rhodamine B through photocatalytic and adsorption treatments," *Journal of Environmental Management*, vol. 85, no. 4, pp. 956–964, 2007.

[5] P. Tao, Y. Xu, C. Song et al., "A novel strategy for the removal of rhodamine B (RhB) dye from wastewater by coal-based carbon membranes coupled with the electric field," *Separation and Purification Technology*, vol. 179, pp. 175–183, 2017.

[6] X. X. Ou, C. Wang, Y. Su, F. J. Zhang, G. J. Yang, and L. Y. Wang, "Degradation of rhodamine B in aqueous solution by Fenton's reagent," *Advanced Materials Research*, vol. 233-235, pp. 737–740, 2011.

[7] T. A. Khan, S. Dahiya, and I. Ali, "Use of kaolinite as adsorbent: equilibrium, dynamics and thermodynamic studies on the adsorption of rhodamine B from aqueous solution," *Applied Clay Science*, vol. 6, pp. 58–66, 2012.

[8] Z. L. Cheng, Y. X. Li, and Z. Liu, "Study on adsorption of rhodamine B onto beta zeolites by tuning SiO_2/Al_2O_3 ratio," *Ecotoxicology and Environmental Safety*, vol. 148, pp. 585–592, 2018.

[9] S. K. Giri and N. N. Das, "Visible light induced photocatalytic decolourisation of rhodamine B by magnetite nanoparticles synthesised using recovered iron from waste iron ore tailing," *Desalination and Water Treatment*, vol. 57, no. 2, pp. 900–907, 2016.

[10] E. Bladev, D. Mubarakalia, A. Iiavarasi, D. Pandiaraj, K. A. Sheik Syed Ishackc, and N. Thajuddina, "Degradation of synthetic dye, rhodamine B to environmentally non-toxic products using microalgae," *Colloids and Surfaces B: Biointerfaces*, vol. 105, pp. 207–214, 2013.

[11] L. C. A. Oliveira, R. V. R. A. Rios, J. D. Fabris, V. Garg, K. Sapag, and R. M. Lago, "Activated carbon/iron oxide magnetic composites for the adsorption of contaminants in water," *Carbon*, vol. 40, no. 12, pp. 2177–2183, 2002.

[12] T. Rohani and M. S. Seyedghasemi, "Application of surfactant-coated magnetic zeolite NAA as a new sorbent to remove Safranin O dye from aqueous solutions," *Bulgarian Chemical Communications*, vol. 323, 2017.

[13] S. Lee, K. Lee, and J. Park, "Simultaneous removal of Cd and Cr(VI) using Fe-loaded zeolite," *Journal of Environmental Engineering*, vol. 132, no. 4, pp. 445–450, 2006.

[14] D. A. Fungaro, M. Yamaura, and T. E. M. Carvalho, "Adsorption of anionic dyes from aqueous solution on zeolite from fly ash-iron oxide magnetic nanocomposite," *Journal of Atomic and Molecular Sciences*, vol. 2, no. 4, pp. 305–316, 2011.

[15] B. Dutta, S. Jana, A. Bhattacharjee, P. Gütlich, S. Iijima, and S. Koner, "γ-Fe_2O_3 nanoparticle in NaY-zeolite matrix: preparation, characterization, and heterogeneous catalytic epoxidation of olefins," *Inorganica Chimica Acta*, vol. 363, no. 4, pp. 696–704, 2010.

[16] C. B. Vidal, G. S. C. Raulino, A. L. Barros et al., "BTEX removal from aqueous solutions by HDTMA-modified Y zeolite," *Journal of Environmental Management*, vol. 112, pp. 178–185, 2012.

[17] A. A. Rajabi, Y. Yamini, M. Faraji, and F. Nourmohammadian, "Modified magnetite nanoparticles with cetyltrimethylammonium bromide as superior adsorbent for rapid removal of the disperse dyes from wastewater of textile companies," *Nanochemistry Research*, vol. 1, pp. 49–56, 2016.

[18] J. Dai, X. Xiao, S. Duan et al., "Synthesis of novel microporous nanocomposites of ZIF-8 on multiwalled carbon nanotubes for adsorptive removing benzoic acid from water," *Chemical Engineering Journal*, vol. 331, pp. 64–74, 2018.

[19] S. Zhang, M. Zeng, J. Li, J. Li, J. Xu, and X. Wang, "Porous magnetic carbon sheets from biomass as an adsorbent for the fast removal of organic pollutants from aqueous solution," *Journal of Materials Chemistry A*, vol. 2, no. 12, pp. 4391–4397, 2014.

[20] S. A. Abdulkareem, E. Muzenda, A. S. Afolabi, and J. Kabuba, "Treatment of clinoptilolite as an adsorbent for the removal of copper ion from synthetic wastewater solution," *Arabian Journal for Science and Engineering*, vol. 38, no. 9, pp. 2263–2272, 2013.

[21] M. Jain, V. K. Garg, and K. Kadirvelu, "Adsorption of hexavalent chromium from aqueous medium onto carbonaceous

adsorbents prepared from waste biomass," *Journal of Environmental Management*, vol. 91, no. 4, pp. 949–957, 2010.

[22] R. Mahmoud, S. Abdel Moaty, F. Mohamed, and A. Farghali, "Comparative study of single and multiple pollutants system using Ti–Fe chitosan LDH adsorbent with high performance in wastewater treatment," *Journal of Chemical and Engineering Data*, vol. 62, no. 11, pp. 3703–3722, 2017.

[23] M. I. El-Khaiary and G. F. Malash, "Common data analysis errors in batch adsorption studies," *Hydrometallurgy*, vol. 105, no. 3-4, pp. 314–320, 2011.

[24] B. Subramanyam and A. Das, "Linearised and non-linearised isotherm models optimization analysis by error functions and statistical means," *Journal of Environmental Health Science and Engineering*, vol. 12, no. 1, p. 92, 2014.

[25] L. Zhou, Q. Yu, Y. Cui et al., "Adsorption properties of activated carbon from reed with a high adsorption capacity," *Ecological Engineering*, vol. 102, pp. 443–450, 2017.

[26] C. Lei, Y. Y. Hua, and M. Z. He, "Adsorption characteristics of triclosan from aqueous solution onto cetylpyridinium bromide (CPB) modified zeolites," *Chemical Engineering Journal*, vol. 219, pp. 361–370, 2013.

[27] G. F. Malash and M. I. El-Khaiary, "Piecewise linear regression: a statistical method for the analysis of experimental adsorption data by the intraparticle-diffusion models," *Chemical Engineering Journal*, vol. 163, no. 3, pp. 256–263, 2010.

[28] D. Guaya, C. Valderrama, A. Farran, and J. L. Cortina, "Modification of a natural zeolite with Fe(III) for simultaneous phosphate and ammonium removal from aqueous solutions," *Journal of Chemical Technology and Biotechnology*, vol. 91, no. 6, pp. 1737–1746, 2016.

[29] K. G. Bhattacharyya, S. SenGupta, and G. K. Sarma, "Interactions of the dye, rhodamine B with kaolinite and montmorillonite in water," *Applied Clay Science*, vol. 99, pp. 7–17, 2014.

[30] H. Liu, X. Ren, and L. Chen, "Synthesis and characterization of magnetic metal–organic framework for the adsorptive removal of rhodamine B from aqueous solution," *Journal of Industrial and Engineering Chemistry*, vol. 34, pp. 278–285, 2016.

[31] B. O. Haglund, L. O. Sundelof, S. M. Upadrashta, and D. E. Wurster, "Effect of SDS micelles on rhodamine-B diffusion in hydrogels," *Journal of Chemical Education*, vol. 73, no. 9, p. 889, 1996.

[32] N. Van Suc and D. Kim Chi, "Removal of rhodamine B from aqueous solution via adsorption onto microwave-activated rice husk ash," *Journal of Dispersion Science and Technology*, vol. 38, no. 2, pp. 216–222, 2017.

[33] S. X. Zhang, X. S. Chai, and D. G. Barnes, "Determination of critical micelle concentration of surfactants by headspace gas chromatography," *Journal of Surfactants and Detergents*, vol. 20, no. 6, pp. 1395–1400, 2017.

[34] V. K. Paruchuri, A. V. Nguyen, and J. D. Miller, "Zeta-potentials of self-assembled surface micelles of ionic surfactants adsorbed at hydrophobic graphite surfaces," *Colloids and Surfaces A: Physicochemical and Engineering Aspects*, vol. 250, no. 1–3, pp. 519–526, 2004.

[35] X. Gao and J. Chorover, "Adsorption of sodium dodecyl sulfate (SDS) at ZnSe and alpha-Fe_2O_3 surfaces: combining infrared spectroscopy and batch uptake studies," *Journal of Colloid and Interface Science*, vol. 348, no. 1, pp. 167–176, 2010.

[36] S. Shariati, M. Faraji, Y. Yamini, and A. A. Rajabi, "Fe_3O_4 magnetic nanoparticles modified with sodium dodecyl sulfate for removal of safranin O dye from aqueous solutions," *Desalination*, vol. 270, no. 1–3, pp. 160–165, 2011.

[37] M. I. Mohammed, A. A. Abdul Razak, and D. A. Hussein Al-Timimi, "Modified multiwalled carbon nanotubes for treatment of some organic dyes in wastewater," *Advances in Materials Science and Engineering*, vol. 2014, Article ID 201052, 10 pages, 2014.

[38] M. I. Mohammed and S. Baytak, "Synthesis of bentonite–carbon nanotube nanocomposite and its adsorption of rhodamine dye from water," *Arabian Journal for Science and Engineering*, vol. 41, no. 12, pp. 4775–4785, 2016.

[39] S. M. Al-Rashed and A. A. Al-Gaid, "Kinetic and thermodynamic studies on the adsorption behavior of rhodamine B dye on Duolite C-20 resin," *Journal of Saudi Chemical Society*, vol. 16, no. 2, pp. 209–215, 2012.

[40] T. A. Khan, S. Sharma, and I. Ali, "Adsorption of rhodamine B dye from aqueous solution onto acid activated mango (*Magnifera indica*) leaf powder: equilibrium, kinetic and thermodynamic studies," *Journal of Toxicology and Environmental Health, Part A*, vol. 3, pp. 286–297, 2011.

[41] X. J. Xiong, X. J. Meng, and T. L. Zheng, "Biosorption of C.I. direct b 199 from aqueous solution by nonviable *Aspergillus niger*," *Journal of Hazardous Materials*, vol. 175, no. 1–3, pp. 241–246, 2010.

[42] M. Schwaab, E. Steffani, E. Barbosa-Coutinho, and J. B. Severo Júnior, "Critical analysis of adsorption/diffusion modelling as a function of time square root," *Chemical Engineering Science*, vol. 173, pp. 179–186, 2017.